Vol 12 No 3, March 2003
1009-1963/2003/12(03)/0275-12

Chinese Physics

© 2003 Chin. Phys. Soc.
and IOP Publishing Ltd

Silane photoabsorption spectra near the Si 2p thresholds: the geometry of Si 2p excited SiH_4^{**}*

Zhang Wei-Hua(张卫华)[a], Xu Ru-Qing(许如清)[a], and Li Jia-Ming(李家明)[a,b]

[a] *Department of Physics, Center of Atom and Molecular Nanosciences, Tsinghua University, Beijing* 100084, *China*

[b] *Institute of Physics, Chinese Academy of Sciences, Beijing* 100080, *China*

(Received 12 July 2002; revised manuscript received 4 December 2002)

Based on the multiple-scattering self-consistent-field method, we have studied the photoabsorption spectra near the Si 2p thresholds of silane. According to our calculations, the clear assignments of the inner-shell photoabsorption spectra are provided. In comparison with the high-resolution experimental spectra, the geometric structure of the Si 2p-excited SiH_4^{**} is recommended to be of a C_{2v} symmetry. More specifically, the Si 2p-excited SiH_4^{**} have two bond lengths of 2.50 a.u. and another two bond lengths of 2.77 a.u., and the corresponding two bond angles are 104.0° and 112.5° respectively.

Keywords: molecular geometry, inner-shell photoabsorption, near-threshold structure, silane
PACC: 3310, 3370

1. Introduction

The inner-shell photoabsorption spectra (i.e., near-threshold structures) provide a significant probe to investigate the electronic structures of molecules and the breaking of molecular bonds due to local excitations. There has been increased interest in recent years on the silane (SiH_4) molecule, for it is widely used in semiconductor industry for the fabrication of materials such as hydrogenated amorphous silicon thin films.[1] Recently, high-resolution core-excited photoabsorption spectra near the Si 2p ionization thresholds of silane have been reported.[2–6] In this paper, we calculate the Si 2p photoabsorption spectra of silane based on the multiple-scattering self-consistent-field method[7–12] which has been applied successfully to some molecules.[13–17] The spin–orbit interaction and the molecular-field effects for the Si 2p core orbitals are also taken into account in our investigation. Comparing with high-resolution experimental spectra,[2,6] we can recommend the geometry of the Si 2p excited SiH_4^{**} to be of a C_{2v} symmetry instead of a T_d symmetry, which is consistent with the previous determination of the molecular geometry of the Si 2p-excited SiH_4^{**} based on the multi-mode Frank–Condon analysis of the vibrationally resolved inner-shell photoabsorption spectra.[6] More specifically, the Si 2p-excited SiH_4^{**} have two bond lengths of 2.50 a.u. and another two bond lengths of 2.77 a.u., and the corresponding two bond angles are 104.0° and 112.5° respectively. It is interesting to note that the core-excited CH_4^{**} is of a C_{3v} symmetry in our previous study.[15] According to our calculations, we provide new assignments for the inner-shell photoabsorption spectra of SiH_4, which are different from the earlier reports.[2,6] Especially, the ratio of the oscillator strengths for transitions from $2p_{1/2}$ to those from $2p_{3/2}$ in Ref.[2] apparently deviates from the statistical ratio 1/2, while our calculated ratio is about 1/2. In section 2, we will report our theoretical method and calculated results in detail. In section 3, the following points will be discussed: (i) determining molecular geometries from the inner-shell photoabsorption spectra involving non-diffusive molecular orbitals and Rydberg orbitals; (ii) possible applications of near-threshold structures, such as the determination of the orientation of molecules in a specific environment; (iii) our calculated wavefunctions can serve as a good starting point for further theoretical treatments.

*Project supported by the Ministry of Science and Technology of China, by the National Natural Science Foundation of China, Ministry of Education of China, National High-Technology Inertial Confinement Fusion Committee of China and Chinese Research Association of Atomic & Molecular Data.

2. Theoretical method and calculated results

The multiple-scattering self-consistent field (MSSCF or MS-X_α) method[7–12] is employed in our present work. Based on a trial charge density of molecules, a muffin-tin trial molecular potential $V^{\rm mol}$ with the symmetry of molecular point group is constructed:

$$V^{\rm mol} = \begin{cases} V(r_i) & \text{within the atomic spheres } i, \\ \overline{V} & \text{in the interstitial region,} \\ V(r) & \text{outside the outer sphere.} \end{cases}$$

We can then calculate the occupied molecular orbitals (MOs). The calculated MOs serve to construct the charge density of the molecule and then a new trial molecular potential. With this process going on, self-consistent iterations are undertaken until a certain precision is met. Thus we obtain a self-consistent-field (SCF) molecular potential $V_{\rm scf}^{\rm mol}$ and thereafter use it to calculate all the MOs, including non-diffusive molecular orbitals (NMOs; i.e., localized bonding, antibonding, and non-bonding molecular orbitals), Rydberg molecular orbitals (RMOs), and adjacent continuum molecular orbitals (CMOs).[10,25,30,31] In particular, the molecular wavefunctions can be expressed in the following forms:

(1) Within the atomic spheres, we have

$$\psi^{\tau\sigma} = \sum_{a\neq 1}\sum_{l\in L_a}\sum_{\delta} C_{a,l}^{\delta} R_l(r_a) \times \sum_{i\in P_a}\sum_{\overline{m}} \mathcal{X}_{l\overline{m}}^{\tau\sigma,\delta}(i) y_{l\overline{m}}(\boldsymbol{r}_i), \quad (1)$$

where r_a is the radial distance from the atomic centre a, $R_l(r_a)$ is an l-partial-wave radial wavefunction that satisfies the Schrödinger equation of the central potential and is normalized within the atomic sphere. The symbol τ represents an irreducible representation of the molecular point group and σ is the index for the degeneracy in the τ-irreducible representation. P_a is the set of the equivalent atomic spheres. In each atomic sphere i belonging to P_a, the wavefunction is expanded into partial wave l with $L_a = \{l : l \leq l_a\}$. $Y_{l\overline{m}}$ is the real spherical harmonic. The symmetric adapted coefficient $\mathcal{X}_{l\overline{m}}^{\tau\sigma,\delta}$ is the normalized projection coefficient of the spherical harmonic in which $l\overline{m}$ is changed into the symmetric representation $\tau\sigma$. The index δ represents the repeating number of projection.

(2) In the interstitial region, we have

$$\psi^{\tau\sigma} = \sum_{a\neq 1}\sum_{l\in L_a}\sum_{\delta} B_{a,l}^{\delta} n_l(kr_a) \times \sum_{i\in P_a, i\neq 1}\sum_{\overline{m}} \mathcal{X}_{l\overline{m}}^{\tau\sigma,\delta}(i) y_{l\overline{m}}(\boldsymbol{r}_i) + \sum_{l\in L_1}\sum_{\delta} B_{1,l}^{\delta} j_l(kr_1) \times \sum_{\overline{m}} \mathcal{X}_{l\overline{m}}^{\tau\sigma,\delta}(1) y_{l\overline{m}}(\boldsymbol{r}_1), \quad (2)$$

where r_1 is the radial distance with respect to the centre of the outer sphere. The j_l and n_l are the spherical Bessel function and spherical Neumann function respectively. k is the wavenumber with respect to the interstitial constant potential.

(3) Outside the outer sphere, we have

$$\psi^{\tau\sigma} = \sum_{l\in L_1}\sum_{\delta} C_{1,l}^{\delta} F_l(r_1) \sum_{\overline{m}} \mathcal{X}_{l\overline{m}}^{\tau\sigma,\delta}(1) y_{l\overline{m}}(\boldsymbol{r}_1), \quad (3)$$

where $F_l(r_1)$ is the l-wave radial wavefunction. All the expansion coefficients $C_{a,l}^{\delta}$ and $B_{a,l}^{\delta}$ are determined by matching the boundary conditions.[10,25,30,31] NMOs can be denoted as $m\tau$, where m represents the mth molecular orbital in the irreducible representation τ. RMOs (or their adjacent CMOs), in the irreducible representation τ, can be denoted as $nl\tau$ ($\epsilon l\tau$), where n (ϵ) is the principal quantum number (or the corresponding positive orbital energy), and l is the major angular momentum in the partial-wave expansion(L_1) outside the outer sphere. These RMOs (CMOs) can be treated as a channel ($l\tau$) within the framework of the quantum-defect theory (QDT).[16,18–21] With the calculated MOs, we can study molecular photoabsorption processes by calculating their transition matrix elements and corresponding oscillator strength densities. We have employed this method to study the electronic structures of molecular Rydberg states[16,22–29] and the photoabsorption spectra,[13–15,17,30–35] which are in good agreement with the experimental data.

A molecular inner-shell photoabsorption process is a transition from an initial core orbital into a final unoccupied NMO, RMO or CMO. The excited molecule in its final state generally consists of an excited electron and a residual ion which has a highly localized inner-shell hole in the corresponding atom of the molecule. The attractive effect due to the hole can be taken into account by adopting a "$Z+1$ model potential".[13,14] In our calculations, the $Z+1$ model potential is obtained by calculating the molecular SCF potential based on the electronic configuration with an inner-shell hole in the corresponding atom

of the molecule and an electron occupying the lowest unoccupied molecular orbital (LUMO). With the $Z+1$ model molecular potential and the corresponding wavefunctions, we can calculate the oscillator strength $f_{fi} = 2\omega_{fi} |\langle f \| D \| i \rangle|^2$ for the NMO and RMO, as well as the oscillator strength density $\mathrm{d}f_{fi}/\mathrm{d}\epsilon_f$ for CMO. Here, the transition energy ω_{fi} (in units of a.u.) is taken to be $\omega_{fi} = I + \epsilon_f$, where the threshold I is taken from the experimental value, and the final orbital energy ϵ_f is calculated based on the $Z+1$ model potential. Note that for the $l \neq 0$ core orbitals, the spin–orbit interaction and the molecular-field effects may cause splittings of the ionization thresholds I,[36,37] which have been considered in our investigation.

In our calculations, all the RMOs and CMOs can be treated in a unified manner within the framework of QDT.[10,25,30,31] According to QDT, channel quantum defects, channel wavefunctions at short ranges and channel oscillator strength densities are smoothly energy-dependent within the neighbourhood of threshold, i.e., so-called channel characters.[16,17] Therefore, for a specific channel α, we only need to calculate the orbital energies $\epsilon_{n,\alpha}$ and the corresponding electronic oscillator strength densities $(\mathrm{d}f/\mathrm{d}\epsilon)_{n,\alpha}$ for a few RMOs and a few CMOs near the threshold. Then, for any high n Rydberg orbitals, their $\epsilon_{n,\alpha}$ and $(\mathrm{d}f/\mathrm{d}\epsilon)_{n,\alpha}$ can be obtained based on the channel characters through interpolations. More specifically, we can obtain the electronic oscillator strength $f_{n,\alpha}$ from the oscillator strength density $(\mathrm{d}f/\mathrm{d}\epsilon)_{n,\alpha}$ for any high n Rydberg orbital by the following formula (in a.u.)

$$\left(\frac{\mathrm{d}f}{\mathrm{d}\epsilon}\right)_{n,\alpha} = f_{n,\alpha} \left(\frac{\mathrm{d}N}{\mathrm{d}\epsilon}\right)_{n,\alpha},$$

where $(\mathrm{d}N/\mathrm{d}\epsilon)_{n,\alpha} = \nu_{n,\alpha}^3$ is the density of states. The excited orbital energy $\epsilon_{n,\alpha} = -\dfrac{1}{2\nu_{n,\alpha}^2}$ with $\nu_{n,\alpha} = n - \mu_\alpha$ (μ_α is the quantum defect for the channel α).

The electronic configuration of the ground state SiH_4 with a T_d symmetry can be written as

$$(1a_1)^2\,(2a_1)^2\,(1t_2)^6\,(3a_1)^2\,(2t_2)^6(4a_1^*)^0\,(3t_2^*)^0$$

with $1a_1$, $2a_1$ and $1t_2$ corresponding to 1s, 2s and 2p core orbitals in the Si atom of silane respectively. The Si–H bonding orbitals are the $3a_1$ and the triply degenerate $2t_2$, i.e., the highest occupied molecular orbital (HOMO). There exist the unoccupied antibonding MOs: $4a_1^*$(LUMO) and $3t_2^*$. They can be regarded as precursor orbitals[26–29] $4\mathrm{s}a_1(4a_1^*)$ and $3\mathrm{d}t_2$ $(3t_2^*)$, since they are also the initial orbitals of $n\mathrm{s}a_1$ and $n\mathrm{d}t_2$ Rydberg series (channels) respectively. In the inner-shell photoabsorption process of SiH_4, according to the selection rule, an electron is excited from the Si 2p core orbitals into unoccupied excited MOs ($n\mathrm{s}a_1$, $n\mathrm{p}t_2$, $n\mathrm{d}t_2$, $n\mathrm{d}e$) for the $\mathrm{s}a_1$, $\mathrm{p}t_2$, $\mathrm{d}t_2$ and $\mathrm{d}e$ channels respectively. Considering the spin–orbit interaction and molecular-field effects, the Si 2p core orbitals will split into three orbitals (see the appendix). If we adopt the S_4 axis of the T_d point group as the $\hat{z}$ axis, these three orbitals could be denoted as $2\mathrm{p}_{J,|M_J|}$, where J denotes the total angular momentum and M_J is the projection of the total angular momentum on the $\hat{z}$ axis:

$$\begin{aligned}
|2\mathrm{p}_{1/2,1/2}{}_-^+\rangle =& \frac{1}{\sqrt{3}}|2\mathrm{p}_{x\beta}^{\alpha}\rangle \\
& \mp \frac{\mathrm{i}}{\sqrt{3}}|2\mathrm{p}_{y\beta}^{\alpha}\rangle \pm \frac{1}{\sqrt{3}}|2\mathrm{p}_{z\alpha}^{\beta}\rangle, \\
|2\mathrm{p}_{3/2,1/2}{}_-^+\rangle =& -\frac{1}{\sqrt{6}}|2\mathrm{p}_{x\beta}^{\alpha}\rangle \\
& \pm \frac{\mathrm{i}}{\sqrt{6}}|2\mathrm{p}_{y\beta}^{\alpha}\rangle \pm \sqrt{\frac{2}{3}}|2\mathrm{p}_{z\alpha}^{\beta}\rangle, \\
|2\mathrm{p}_{3/2,3/2}{}_-^+\rangle =& \frac{1}{\sqrt{2}}|2\mathrm{p}_{x\beta}^{\alpha}\rangle \pm \frac{\mathrm{i}}{\sqrt{2}}|2\mathrm{p}_{y\beta}^{\alpha}\rangle. \qquad (4)
\end{aligned}$$

Here $2\mathrm{p}_x$, $2\mathrm{p}_y$ and $2\mathrm{p}_z$ are Cartesian orbitals, and α and β denote the up and down of the electron spin respectively. Each of the three core orbitals are doubly degenerate due to different spin orientations. Note that the $2\mathrm{p}_{3/2,1/2}$ and $2\mathrm{p}_{3/2,3/2}$ are still degenerate orbitals with a T_d symmetry. Thus, the Si 2p ionization thresholds are 107.95 eV for $2\mathrm{p}_{1/2,1/2}$ and 107.31 eV for both $2\mathrm{p}_{3/2,1/2}$ and $2\mathrm{p}_{3/2,3/2}$.[4] The calculated orbital energies $\epsilon_{n,\alpha}$, quantum defects μ_α, their corresponding excitation energies $E_{n,\alpha}^{\mathrm{ex}}$, oscillator strengths $f_{n,\alpha}$ and oscillator strength densities $(\mathrm{d}f/\mathrm{d}\epsilon)_{n,\alpha}$ from the Si $2\mathrm{p}_{1/2,1/2}$, $2\mathrm{p}_{3/2,1/2}$ and $2\mathrm{p}_{3/2,3/2}$ core orbitals respectively are listed in Table 1.

Table 1. Calculated quantum defect (μ_α), orbital energy ($\epsilon_{n,\alpha}$, in units a.u), and the corresponding excitation energy ($E^{ex}_{n,\alpha}$, in eV), oscillator strength ($f_{n,\alpha}$) and oscillator strength density ($(\mathrm{d}f/\mathrm{d}\epsilon)_{n,\alpha}$, in a.u.$^{-1}$) from the $2p_{1/2,1/2}$, $2p_{3/2,1/2}$ and $2p_{3/2,3/2}$ core orbitals with a T_d symmetry.

channel			$2p_{1/2,1/2}$			$2p_{3/2,1/2}$			$2p_{3/2,3/2}$	
α	μ_α	$\epsilon_{n,\alpha}$ [a]	$E^{ex}_{n,\alpha}$ [b]	$f_{n,\alpha}$	$\left(\frac{\mathrm{d}f}{\mathrm{d}\epsilon}\right)_{n,\alpha}$ [c]	$E^{ex}_{n,\alpha}$	$f_{n,\alpha}$	$\left(\frac{\mathrm{d}f}{\mathrm{d}\epsilon}\right)_{n,\alpha}$	$f_{n,\alpha}$	$\left(\frac{\mathrm{d}f}{\mathrm{d}\epsilon}\right)_{n,\alpha}$
				$a[b]$	$a[b]$		$a[b]$	$a[b]$	$a[b]$	$a[b]$
$4sa_1$	2.04	–0.130	104.42	4.9[–3]	3.7[–2]	103.78	4.8[–3]	3.7[–2]	4.8[–3]	3.7[–2]
$5sa_1$	2.06	–0.058	106.38	1.5[–3]	3.9[–2]	105.74	1.5[–3]	3.9[–2]	1.5[–3]	3.9[–2]
$6sa_1$	2.09	–0.033	107.06	6.0[–4]	3.6[–2]	106.42	5.9[–4]	3.6[–2]	5.9[–4]	3.6[–2]
$7sa_1$	2.11	–0.021	107.38	2.9[–4]	3.4[–2]	106.74	2.9[–4]	3.4[–2]	2.9[–4]	3.4[–2]
ϵsa_1	2.16	0.003	108.02		3.1[–2]	107.38		3.1[–2]		3.1[–2]
$4pt_2$	1.52	–0.081	105.74	4.9[–5]	7.4[–4]	105.10	4.8[–5]	7.4[–4]	4.8[–5]	7.4[–4]
$5pt_2$	1.50	–0.041	106.84	2.7[–6]	1.2[–4]	106.20	2.7[–6]	1.2[–4]	2.7[–6]	1.2[–4]
$6pt_2$	1.49	–0.025	107.28	2.4[–7]	2.2[–5]	106.64	2.3[–7]	2.1[–5]	2.3[–7]	2.1[–5]
$7pt_2$	1.49	–0.016	107.50	1.4[–8]	2.4[–6]	106.86	1.4[–8]	2.4[–6]	1.4[–8]	2.4[–6]
ϵpt_2	1.48	0.003	108.02		3.3[–5]	107.38		3.3[–5]		3.3[–5]
$3dt_2$	1.07	–0.134	104.30	2.2[–2]	1.6[–1]	103.66	2.2[–2]	1.6[–1]	2.2[–2]	1.6[–1]
$4dt_2$	0.76	–0.048	106.66	1.5[–3]	5.1[–2]	106.02	1.5[–3]	5.1[–2]	1.5[–3]	5.1[–2]
$5dt_2$	0.73	–0.027	107.20	6.5[–4]	5.0[–2]	106.56	6.4[–4]	5.0[–2]	6.4[–4]	5.0[–2]
$6dt_2$	0.72	–0.018	107.46	3.4[–4]	5.0[–2]	106.82	3.4[–4]	5.0[–2]	3.4[–4]	5.0[–2]
$7dt_2$	0.71	–0.013	107.61	2.0[–4]	5.0[–2]	106.97	2.0[–4]	5.0[–2]	2.0[–4]	5.0[–2]
ϵdt_2	0.70	0.003	108.02		5.1[–2]	107.38		5.1[–2]		5.1[–2]
$3de$	0.42	–0.075	105.90	7.7[–3]	1.3[–1]	105.26	1.1[–2]	2.0[–1]	3.8[–3]	6.6[–2]
$4de$	0.48	–0.040	106.85	2.6[–3]	1.1[–1]	106.21	3.9[–3]	1.7[–1]	1.3[–3]	5.6[–2]
$5de$	0.49	–0.025	107.28	1.1[–3]	1.0[–1]	106.64	1.7[–3]	1.6[–1]	5.7[–4]	5.2[–2]
$6de$	0.49	–0.016	107.50	6.1[–4]	1.0[–1]	106.86	9.0[–4]	1.5[–1]	3.0[–4]	5.0[–2]
$7de$	0.49	–0.012	107.63	3.6[–4]	9.9[–2]	106.99	5.4[–4]	1.5[–1]	1.8[–4]	4.9[–2]
ϵde	0.50	0.003	108.02		9.5[–2]	107.38		1.4[–1]		4.7[–2]

[a] Orbital energy of RMO is $\epsilon_{n,\alpha} = -1/(2\nu^2_{n,\alpha})$ with $\nu_{n,\alpha} = n - \mu_\alpha$.

[b] Excitation energy is $E^{ex}_{n,\alpha} = I + \epsilon_{n,\alpha}$, where I is the ionization threshold. $I = 107.95$eV for $2p_{1/2,1/2}$ and $I = 107.31$eV for both $2p_{3/2,1/2}$ and $2p_{3/2,3/2}$.

[c] Oscillator strength density is $(\mathrm{d}f/\mathrm{d}\epsilon)_{n,\alpha} = \nu^3_{n,\alpha} f_{n,\alpha}$.

$a[b] \equiv a \times 10^b$.

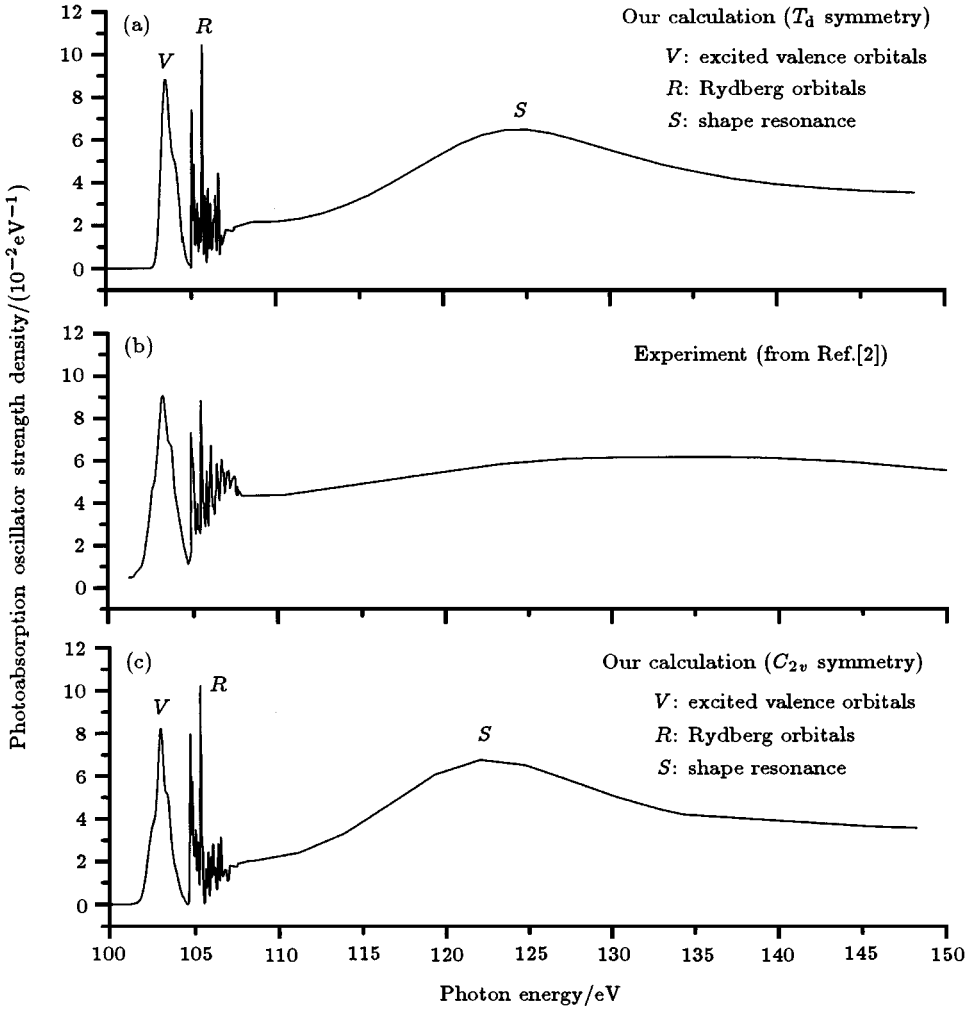


Fig.1. Si 2p photoabsorption spectra of SiH_4: (a) theoretical result with a T_d symmetry; (b) experimental spectra, taken from Ref.[2]; (c) theoretical result with a C_{2v} symmetry. $\sigma(10^{-18}\mathrm{cm}^2) = 1.0975 \times 10^2 \frac{\mathrm{d}f}{\mathrm{d}E}$ (eV^{-1}).

Figure 1(a) displays our theoretical photoabsorption spectra of silane with a T_d symmetry. In comparison with the experimental spectra, we should take into account the following three points: (1) For CMOs, we directly plot the calculated oscillator strength densities in the graph. (2) For the higher RMOs close to the threshold, the density of states $N^2_{n,\alpha} = \nu^3_{n,\alpha}$ (in units of a.u.$^{-1}$) is so great that one cannot resolve adjacent states in experimental measurements. We then define the oscillator strength density at energy E as $\mathrm{d}f/\mathrm{d}E = \sum_\alpha \left(\frac{\mathrm{d}f}{\mathrm{d}\epsilon}\right)_{n,\alpha} = \sum_\alpha f_{n,\alpha} N^2_{n,\alpha}$, where the sum is taken over all the Rydberg series (i.e. all α channels). E is the average energy of the relevant Rydberg states in the same manifold (i.e. with the similar $\nu_{n,\alpha}$). (3) For NMOs and the lower RMOs, the energy separation between two adjacent states is greater than the experimental resolution. We define the oscillator strength density of the electron state $\epsilon_{n,\alpha}$ as a Gaussian profile with its centre energy at $\epsilon_{n,\alpha}$, its width as ΔE, and the profile area equals $f_{n,\alpha}$. Note that the width ΔE includes the instrumental width and the linewidth due to autoionization, pre-dissociation, and radiative processes. Our calculated oscillator strength of a specific transition is the total electronic oscillator strength for all discrete vibrational levels and the associated photodissociation. If the experimental spectra are vibrationally resolved, we can distribute the oscillator strength of a specific electronic transition according to its vibrational distribution (i.e., the experimental vibrational distribution or the Frank–Condon distribution) with the above-mentioned linewidth. More specifically, the electronic oscillator strength equals the sum of all its vibrational oscillator strengths determined according to its vibrational distribution. For the orbitals belonging to a specific channel, their oscillator strengths have similar vibrational distributions according to the channel

characters.[17]

Figure 1(b) shows the absolute photoabsorption cross section near Si 2p ionization thresholds using the synchrotron radiation source.[2] Based on our calculation, we can identify the experimental spectra clearly. The spectra can be divided into three regions: (1) The valence region: a feature at 103 eV is assigned to the excitations from Si 2p orbitals into unoccupied antibonding orbitals ($4sa_1$ and $3dt_2$), which is different from the assignment $2p\rightarrow\ \sigma^*4s$ and $2p\rightarrow\ \sigma^*(t_2)$ in Ref.[2]. (2) The Rydberg region: above 104.8 eV, the spectral features are caused by Si 2p excitations into four Rydberg series, nsa_1, npt_2, ndt_2 and nde, with their vibrational distribution.[6] Note that the oscillator strengths for transitions to pt_2 channel are negligible (Table 1). According to our calculations, the sharp feature at 105.2 eV is assigned to the excitation $(2p_{3/2,1/2}$ or $2p_{3/2,3/2})^{-1}$ $3de$, which is different from the assignment $2p_{3/2}^{-1}$ $5sa_1$ in Ref.[6] and also different from the assignment $2p\rightarrow5s$ and $2p\rightarrow3d(e)$ in Ref.[2]. The sharp feature at 105.8 eV is assigned to excitations $(2p_{3/2,1/2}$ or $2p_{3/2,3/2})^{-1}$ $5sa_1$ and $2p_{1/2,1/2}^{-1}$ $3de$, which are different from the assignments $2p_{1/2}^{-1}$ $5sa_1$ and $2p_{3/2}^{-1}$ $3de$ in Ref.[6] and also different from the assignments $2p\rightarrow3d(t_2)$ in Ref.[2]. (3) The continuum region: above the Si 2p ionization threshold, the absolute photoabsorption cross section exhibits a broad maximum at about 125 eV. This broad hump is caused by the shape resonance in the dt_2 channel. Since channel interactions (i.e., electron correlations) are not taken into account in our present calculation, our calculated shape resonance peak is sharper than the experimental one. Nevertheless, our theoretical calculation with a T_d symmetry can still provide the assignment for the experimental spectra.

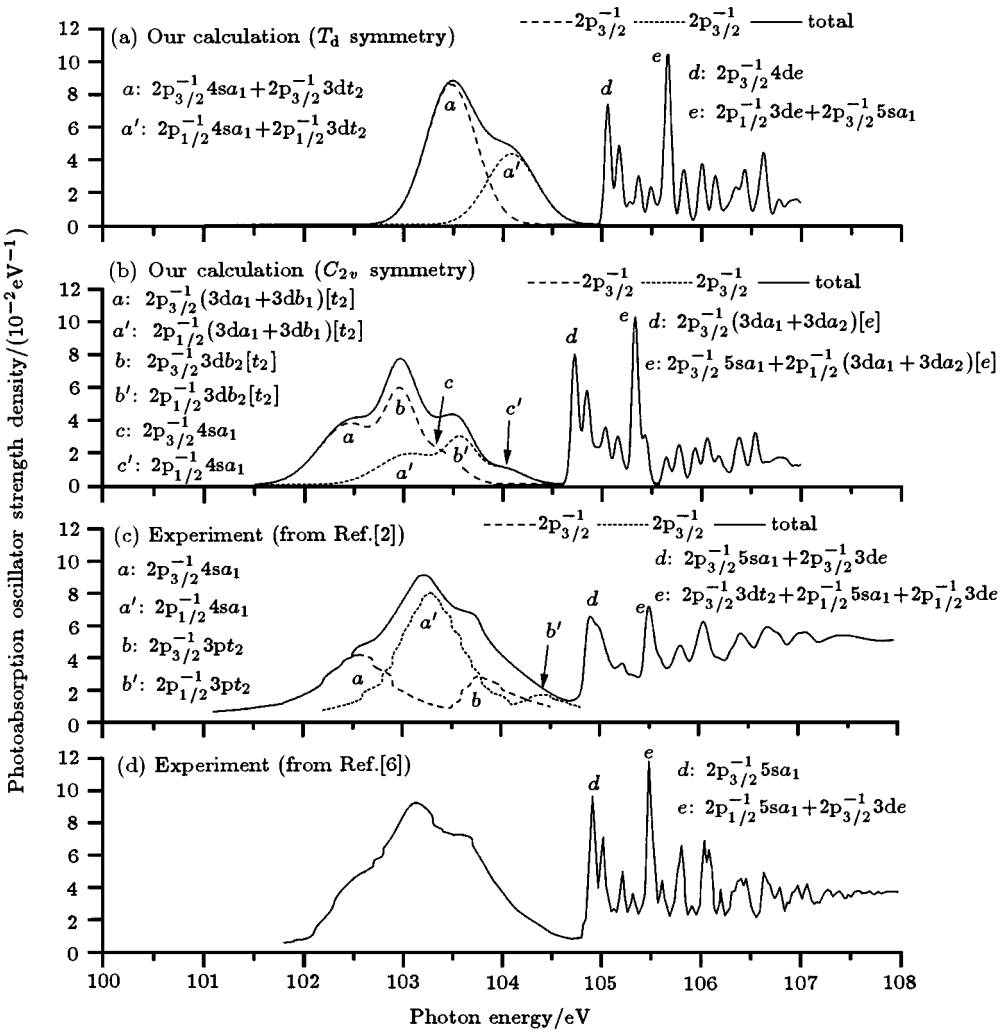


Fig.2. Photoabsorption spectra of SiH_4 below the Si 2p ionization threshold: (a) theoretical result with a T_d symmetry; (b) theoretical result with a C_{2v} symmetry; (c) experimental spectra, taken from Ref.[2]; (d) experimental spectra, taken from Ref.[6]. $\sigma(10^{-18}cm^2) = 1.0975\times10^2\frac{df}{dE}(eV^{-1})$.

With careful examination of the spectra below the threshold, the high-resolution experimental spectra (Figs.2(c) and 2(d)) show three features in the region of 102–104 eV, while our theoretical result with a $T_{\rm d}$ symmetry (Fig.2(a)) only contains two features shifted by about 0.5 eV. Such a discrepancy implies that the Si 2p-excited SiH_4^{**} will not be of a $T_{\rm d}$ symmetry due to Jahn–Teller distortions which would give rise to complicated vibronic structures for the final states of the molecule. Therefore, the final electronic wavefunctions and the corresponding electronic energy levels is sensitive to the molecular geometry. In this paper, we only calculate the total electronic oscillator strengths that are the sum taken over all corresponding vibrational levels. So we should adopt an appropriate geometry where the overlap of the initial and final vibrational wavefunctions is significant. Note that for the initial Si 2p core orbitals, the wavefunctions of different molecular geometries are almost the same, and the spectra corresponding to the energy levels depend mainly on the final geometry of the molecule. Thus, we conduct calculations with various molecular geometries and compare these results with the experimental spectra. Finally, we adopt the geometry of the molecule with a C_{2v} symmetry, with two bond lengths of 2.50 a.u. and two bond lengths of 2.77 a.u. — both values are shorter than that of the $T_{\rm d}$ ground state (2.78 a.u), and the two corresponding bond angles of 104.0° and 112.5° are also different from that (109.5°) of the $T_{\rm d}$ ground state.[6] Taking into consideration the spin–orbit and molecular-field splittings, we can see that the Si 2p core orbitals will split into the following three orbitals with a C_{2v} symmetry (taking the C_2 axis as the $\hat{z}$ axis in our coordinate system):

$$
\begin{aligned}
|(2p_{1/2})\ {}^{+}_{-}\rangle &= 0.55|2p_{x\beta}^{\alpha}\rangle \mp 0.60i|2p_{y\beta}^{\alpha}\rangle \pm 0.58|2p_{z\alpha}^{\beta}\rangle,\\
|(2p_{3/2})_1\ {}^{+}_{-}\rangle &= 0.19|2p_{x\beta}^{\alpha}\rangle \pm 0.77i|2p_{y\beta}^{\alpha}\rangle \pm 0.61|2p_{z\alpha}^{\beta}\rangle, \quad (5)\\
|(2p_{3/2})_2\ {}^{+}_{-}\rangle &= 0.81|2p_{x\beta}^{\alpha}\rangle \pm 0.23i|2p_{y\beta}^{\alpha}\rangle \mp 0.54|2p_{z\alpha}^{\beta}\rangle.
\end{aligned}
$$

These three orbitals correspond to the ionization thresholds of 107.95 eV, 107.32 eV and 107.29 eV respectively, with a splitting of only 0.03 eV between the $(2p_{3/2})_1$ and $(2p_{3/2})_2$ orbitals. Although the resolution of the experimental spectra is 0.015 eV, the intrinsic line-widths of the near-threshold structures (due to ionization and dissociation) are larger than 0.05 eV.[6] Therefore, the splitting of the $(2p_{3/2})_1$ and $(2p_{3/2})_2$ orbitals will be almost unresolved in the observed spectra. However, the molecular field effect can cause a redistribution of the oscillator strengths between the two "$2p_{3/2}$" series, with the corresponding sums unchanged. In Table 2, we list the calculated orbital energy $\epsilon_{n,\alpha}$, quantum defect μ_α, their corresponding excitation energies $E^{\rm ex}_{n,\alpha}$, oscillator strengths $f_{n,\alpha}$ and oscillator strength densities $({\rm d}f/{\rm d}\epsilon)_{n,\alpha}$ from the Si $(2p_{1/2})$, $(2p_{3/2})_1$ and $(2p_{3/2})_2$ core orbitals. Figure 2(b) displays the calculated Si 2p photoabsorption spectra of SiH_4^{**} with a C_{2v} symmetry. Note that with the change of molecular symmetry from $T_{\rm d}$ to C_{2v}, a degenerate orbital of t_2 will split into three orbitals of a_1, b_1 and b_2; a degenerate orbital of e will split into two orbitals of a_1 and a_2. Thus, comparing Fig.2(b) with Fig.2(c), we can explain that the three features in the experimental spectra are caused by the electron excitations from the Si 2p orbital into $4sa_1$, $3da_1$, $3db_1$ and $3db_2$ orbitals with spin–orbit splittings. Our assignments for the spectra are shown in Fig.2(b) and different from Refs.[2] and [6], which will be further discussed in section 3. In comparison with our calculated result with a $T_{\rm d}$ symmetry (Fig.2(a)), the result calculated with a C_{2v} symmetry is in much better agreement with the experimental spectra. This is the clue that the inner-shell photoexcitation from the Si 2p core orbitals into the unoccupied antibonding orbitals, $4a_1^*$ $(4sa_1)$ and $3t_2^*$ $(3dt_2)$, may result in a Jahn–Teller distortion, which changes the geometric structure of SiH_4^{**} into a C_{2v} symmetry.

Table 2. Calculated quantum defect (μ_α), orbital energy ($\epsilon_{n,\alpha}$, in units a.u), and the corresponding excitation energy ($E^{\rm ex}_{n,\alpha}$, in eV), oscillator strength ($f_{n,\alpha}$) and oscillator strength density ($({\rm d}f/{\rm d}\epsilon)_{n,\alpha}$, in a.u.$^{-1}$) from the $(2p_{1/2})$, $(2p_{3/2})_1$ and $(2p_{3/2})_2$ core orbitals with a C_{2v} symmetry.

Channel			$(2p_{1/2})$			$(2p_{3/2})_1$			$(2p_{3/2})_2$		
α	μ_α	$\epsilon^{\rm a)}_{n,\alpha}$	$E^{\rm ex\ b)}_{n,\alpha}$	$f_{n,\alpha}$	$\left(\frac{{\rm d}f}{{\rm d}\epsilon}\right)^{\rm c)}_{n,\alpha}$	$E^{\rm ex}_{n,\alpha}$	$f_{n,\alpha}$	$\left(\frac{{\rm d}f}{{\rm d}\epsilon}\right)_{n,\alpha}$	$E^{\rm ex}_{n,\alpha}$	$f_{n,\alpha}$	$\left(\frac{{\rm d}f}{{\rm d}\epsilon}\right)_{n,\alpha}$
				a[b]	a[b]	a[b]	a[b]	a[b]	a[b]	a[b]	a[b]
$4sa_1$	2.09	–0.137	104.22	4.9[–3]	3.4[–2]	103.59	1.5[–3]	1.1[–2]	103.56	9.1[–3]	6.4[–2]
$5sa_1$	2.15	–0.062	106.28	1.4[–3]	3.3[–2]	105.65	1.1[–3]	2.5[–2]	105.62	1.9[–3]	4.3[–2]
$6sa_1$	2.17	–0.034	107.02	5.8[–4]	3.3[–2]	106.39	4.1[–4]	2.3[–2]	106.36	8.0[–4]	4.5[–2]
$7sa_1$	2.19	–0.022	107.36	2.9[–4]	3.2[–2]	106.73	1.9[–4]	2.1[–2]	106.70	4.1[–4]	4.6[–2]
ϵsa_1	0.31	0.025	108.63		2.5[–2]	108.00		1.1[–2]	107.97		4.2[–2]

Table 2. (*Continued*)

$4pa_1[t_2]$	1.56	–0.084	105.66	4.3[–5]	6.1[–4]	105.03	4.7[–5]	6.8[–4]	105.00	3.7[–5]	5.4[–4]
$5pa_1[t_2]$	1.55	–0.042	106.80	2.2[–5]	9.0[–4]	106.17	2.5[–5]	1.0[–3]	106.14	1.8[–5]	7.5[–4]
$6pa_1[t_2]$	1.55	–0.025	107.26	1.7[–5]	1.5[–3]	106.63	2.0[–5]	1.8[–3]	106.60	1.4[–5]	1.2[–3]
$7pa_1[t_2]$	1.55	–0.017	107.49	1.3[–5]	2.1[–3]	106.86	1.6[–5]	2.6[–3]	106.83	9.9[–6]	1.6[–3]
$\epsilon pa_1[t_2]$	1.54	0.025	108.63		2.3[–2]	108.00		2.8[–2]	107.97		1.6[–2]
$4pb_1[t_2]$	1.56	–0.084	105.66	1.3[–7]	1.9[–6]	105.03	8.3[–8]	1.2[–6]	105.00	1.9[–7]	2.8[–6]
$5pb_1[t_2]$	1.55	–0.042	106.81	1.7[–6]	6.9[–5]	106.18	1.1[–6]	4.5[–5]	106.15	2.5[–6]	1.0[–4]
$6pb_1[t_2]$	1.55	–0.025	107.26	1.8[–6]	1.6[–4]	106.63	1.2[–6]	1.0[–4]	106.60	2.7[–6]	2.4[–4]
$7pb_1[t_2]$	1.54	–0.017	107.49	1.4[–6]	2.3[–4]	106.86	9.1[–7]	1.5[–4]	106.83	2.1[–6]	3.4[–4]
$\epsilon pb_1[t_2]$	1.54	0.025	108.63		8.3[–4]	108.00		5.3[–4]	107.97		1.2[–3]
$4pb_2[t_2]$	1.55	–0.084	105.68	6.3[–5]	9.3[–4]	105.05	8.8[–5]	1.3[–3]	105.02	3.1[–5]	4.5[–4]
$5pb_2[t_2]$	1.54	–0.042	106.81	1.6[–5]	6.5[–4]	106.18	2.2[–5]	9.0[–4]	106.15	7.6[–6]	3.2[–4]
$6pb_2[t_2]$	1.54	–0.025	107.27	6.3[–6]	5.6[–4]	106.64	8.7[–6]	7.7[–4]	106.61	3.1[–6]	2.7[–4]
$7pb_2[t_2]$	1.54	–0.017	107.49	3.2[–6]	5.1[–4]	106.86	4.4[–6]	7.1[–4]	106.83	1.5[–6]	2.5[–4]
$\epsilon pb_2[t_2]$	1.53	0.025	108.63		3.1[–4]	108.00		4.2[–4]	107.97		1.5[–4]
$3da_1[t_2]$	1.29	–0.172	103.28	8.1[–3]	4.0[–2]	102.65	1.2[–2]	5.7[–2]	102.62	3.3[–3]	1.7[–2]
$4da_1[t_2]$	0.79	–0.049	106.63	3.5[–4]	1.1[–2]	106.00	2.8[–4]	9.2[–3]	105.97	4.3[–4]	1.4[–2]
$5da_1[t_2]$	0.76	–0.028	107.19	1.6[–4]	1.2[–2]	106.56	1.3[–4]	9.8[–3]	106.53	1.9[–4]	1.4[–2]
$6da_1[t_2]$	0.75	–0.018	107.46	8.3[–5]	1.2[–2]	106.83	6.9[–5]	1.0[–2]	106.80	9.8[–5]	1.4[–2]
$7da_1[t_2]$	0.75	–0.013	107.60	4.9[–5]	1.2[–2]	106.97	4.1[–5]	1.0[–2]	106.94	5.8[–5]	1.4[–2]
$\epsilon da_1[t_2]$	0.71	0.025	108.63		1.2[–2]	108.00		1.1[–2]	107.97		1.4[–2]
$3db_1[t_2]$	1.29	–0.170	103.32	6.5[–3]	3.3[–2]	102.69	4.2[–3]	2.1[–2]	102.66	9.6[–3]	4.8[–2]
$4db_1[t_2]$	0.80	–0.049	106.62	3.0[–4]	9.7[–3]	105.99	1.9[–4]	6.2[–3]	105.96	4.3[–4]	1.4[–2]
$5db_1[t_2]$	0.77	–0.028	107.19	1.3[–4]	1.0[–2]	106.56	8.7[–5]	6.6[–3]	106.53	2.0[–4]	1.5[–2]
$6db_1[t_2]$	0.76	–0.018	107.46	7.2[–5]	1.0[–2]	106.83	4.7[–5]	6.7[–3]	106.80	1.1[–4]	1.5[–2]
$7db_1[t_2]$	0.75	–0.013	107.60	4.3[–5]	1.1[–2]	106.97	2.8[–5]	6.8[–3]	106.94	6.4[–5]	1.6[–2]
$\epsilon db_1[t_2]$	0.71	0.025	108.63		1.1[–2]	108.00		7.3[–3]	107.97		1.7[–2]
$3db_2[t_2]$	1.19	–0.152	103.81	9.0[–3]	5.3[–2]	103.18	1.2[–2]	7.4[–2]	103.15	4.4[–3]	2.6[–2]
$4db_2[t_2]$	0.79	–0.048	106.63	5.0[–4]	1.7[–2]	106.00	6.9[–4]	2.3[–2]	105.97	2.4[–4]	8.1[–3]
$5db_2[t_2]$	0.76	–0.028	107.19	2.3[–4]	1.7[–2]	106.56	3.1[–4]	2.4[–2]	106.53	1.1[–4]	8.4[–3]
$6db_2[t_2]$	0.75	–0.018	107.46	1.2[–4]	1.8[–2]	106.83	1.7[–4]	2.4[–2]	106.80	5.9[–5]	8.6[–3]
$7db_2[t_2]$	0.74	–0.013	107.60	7.3[–5]	1.8[–2]	106.97	1.0[–4]	2.5[–2]	106.94	3.5[–5]	8.7[–3]
$\epsilon db_2[t_2]$	0.70	0.025	108.63		2.0[–2]	108.00		2.7[–2]	107.97		9.5[–3]
$3da_1[e]$	0.61	–0.087	105.57	5.2[–3]	7.1[–2]	104.94	5.9[–3]	8.0[–2]	104.91	4.3[–3]	5.9[–2]
$4da_1[e]$	0.58	–0.043	106.78	1.1[–3]	4.3[–2]	106.15	1.2[–3]	4.8[–2]	106.12	9.1[–4]	3.6[–2]
$5da_1[e]$	0.57	–0.026	107.26	4.5[–4]	3.9[–2]	106.63	5.0[–4]	4.3[–2]	106.60	3.9[–4]	3.3[–2]
$6da_1[e]$	0.57	–0.017	107.49	2.3[–4]	3.7[–2]	106.86	2.6[–4]	4.1[–2]	106.83	2.0[–4]	3.2[–2]
$7da_1[e]$	0.57	–0.012	107.62	1.4[–4]	3.6[–2]	106.99	1.5[–4]	4.0[–2]	106.96	1.2[–4]	3.2[–2]
$\epsilon da_1[e]$	0.56	0.025	108.63		1.6[–2]	108.00		1.4[–2]	107.97		1.9[–2]
$3da_2[e]$	0.61	–0.087	105.57	5.2[–3]	7.1[–2]	104.94	4.8[–3]	6.6[–2]	104.91	5.5[–3]	7.5[–2]
$4da_2[e]$	0.58	–0.043	106.78	1.1[–3]	4.3[–2]	106.15	1.0[–3]	4.0[–2]	106.12	1.2[–3]	4.6[–2]
$5da_2[e]$	0.57	–0.026	107.26	4.6[–4]	4.0[–2]	106.63	4.3[–4]	3.7[–2]	106.60	4.9[–4]	4.2[–2]
$6da_2[e]$	0.57	–0.017	107.49	2.4[–4]	3.9[–2]	106.86	2.2[–4]	3.6[–2]	106.83	2.6[–4]	4.1[–2]
$7da_2[e]$	0.57	–0.012	107.62	1.4[–4]	3.8[–2]	106.99	1.3[–4]	3.5[–2]	106.96	1.5[–4]	4.1[–2]
$\epsilon da_2[e]$	0.55	0.025	108.63		3.7[–2]	108.00		3.4[–2]	107.97		3.9[–2]

[a] Orbital energy of RMO is $\epsilon_{n,\alpha} = -1/(2\nu_{n,\alpha}^2)$ with $\nu_{n,\alpha} = n - \mu_\alpha$.

[b] Excitation energy is $E_{n,\alpha}^{\rm ex} = I + \epsilon_{n,\alpha}$, where I is the ionization threshold. I =107.95, 107.32 and 107.29 eV for $(2p_{1/2})$, $(2p_{3/2})_1$ and $(2p_{3/2})_2$ respectively.

[c] Oscillator strength density is $(df/d\epsilon)_{n,\alpha} = \nu_{n,\alpha}^3 f_{n,\alpha}$.

$a[b] \equiv a \times 10^b$

3. Discussion

Based on the MSSCF method, we have calculated the inner-shell (Si 2p) photoabsorption spectra for SiH_4, as shown in Figs.1 and 2. Figure 1(a) displays the calculated spectra with a T_d symmetry while Fig.1(c) with a C_{2v} symmetry. Both calculations can provide assignments for the experimental spectra (Fig.1(b)) in a broad energy range of 100–150 eV. As illustrated in section 2, the three regions of the spectra are identified as: (1) The valence region (below 104.5 eV): the feature at 103 eV is caused by excitations into the unoccupied antibonding orbitals $4sa_1$ and $3dt_2$ for a T_d symmetry; or $4sa_1$ and $(3da_1+3db_1+3db_2)[t_2]$ for a C_{2v} symmetry. Here the symbol $[t_2]$ indicates that the nondegenerate orbitals $(da_1+db_1+db_2)$ are split from the degenerate orbital t_2. (2) The Rydberg region (from 104.5 eV to the Si 2p ionization thresholds): the sharp features at 104.8 eV and 105.4 eV are assigned to transitions $((2p_{3/2})_1$ or $(2p_{3/2})_2)^{-1}$ $(3da_1+3da_2)[e]$ and $((2p_{3/2})_1$ or $(2p_{3/2})_2)^{-1}5sa_1+(2p_{1/2})^{-1}$ $(3da_1+3da_2)[e]$ respectively. (3) The continuum region (above the thresholds): the broad hump is caused by shape resonance in the dt_2 channel — the calculated hump is sharper than the experimental one because our method have not taken into account the channel interactions (i.e., electron correlations).

However, with a higher energy resolution, the spectra below the threshold show interesting features: both experimental spectra (Figs.2(c) and 2(d)) show three features in the valence region while the theoretical calculation with a T_d symmetry (Fig.2(a)) only consists of two features shifted by about 0.5 eV. The features in the Rydberg region are also shifted a little by about 0.25 eV in the calculation with a T_d symmetry. On the other hand, the calculated spectra with a C_{2v} symmetry (Fig.2(b)) are in good agreement with the experimental spectra. Furthermore, our calculations can provide clear assignments for the experimental spectra. Our assignments are different from those given in Ref.[6] (Fig.2(d)) and those given in Ref.[2] according to CI calculations. The comparison of our calculated results with the CI calculation results[2] is listed in Table 3. According to our calculations, the total oscillator strength in the broad band is 0.0846, which agrees better with the experimental data (0.09) than that given by CI calculations (0.05) (Table 3). Note that in Ref.[2], the ratio of the oscillator strength $2p_{1/2}^{-1}4sa_1$ to $2p_{3/2}^{-1}4sa_1$ equals 2 which is different from the statistical ratio 1/2, while our calculated ratio of oscillator strengths for transitions from $(2p_{1/2})$ to those from $((2p_{3/2})_1$ and $(2p_{3/2})_2)$ is 0.51 (close to 1/2). The sharp features at about 104.9 eV and 105.6 eV are assigned as transitions into $((2p_{3/2})_1$ or $(2p_{3/2})_2)^{-1}(3da_1+3da_2)[e]$ and $((2p_{3/2})_1$ or $(2p_{3/2})_2)^{-1}$ $5sa_1+(2p_{1/2})^{-1}$ $(3da_1+3da_2)[e]$ respectively, which are different from the assignments of $2p_{3/2}^{-1}$ $5sa_1+2p_{3/2}^{-1}$ $3de$ and $2p_{3/2}^{-1}$ $3dt_2+2p_{1/2}^{-1}$ $5sa_1+2p_{1/2}^{-1}3de$ in Ref.[2] (Fig.2(c)). Meanwhile, our calculated excitation energies agree better with the experimental data than the CI calculation results (Table 3).

Based on our calculated near-threshold absorption spectra, in comparison with the high-resolution experimental spectra, the Si 2p-excited SiH_4^{**} should be of a C_{2v} symmetry with two bond lengths of 2.50 a.u., two bond lengths of 2.77 a.u., and two bond angles of 104.0° and 112.5° respectively. Those are consistent with the results in Ref.[6] (two bond lengths of 2.665 a.u., two bond lengths of 2.688 a.u., and two bond angles of 102.5° and 122.5° respectively). Note that in our calculations, the mass centre of Si 2p-excited SiH_4^{**} is still localized on the Si atom.

Comparing Fig.2(a) with Fig.2(b), we can see that the structures corresponding to transitions into NMOs are sensitive to the geometry of the core-excited molecules. This can be used to determine the geometry of the core-excited molecules, which is a subgroup of the corresponding ground-state symmetry group.[15] Moreover, when the molecules are in a condensed environment, the near-threshold structures involving NMOs still resemble the structures of the corresponding free molecules. We can recognize the molecules by observing the near-threshold structures corresponding to the transitions into NMOs and probe the orientation of the adsorbed molecule according to the selection rule.[13–15,18] Detailed analysis of the near-threshold structures (excitations into NMOs) in order to determine the orientation of the adsorbed SiH_4 molecule will be reported elsewhere.

Table 3. Comparison of the assignments, excitation energies (E_{ex}) and oscillator strengths (f) according to CI calculated results in Ref.[2] and our calculated results.

	Experimental data[a)]		CI calculations[a)]			Our calculations			
	E_{ex}/eV	f_{total}	assignment	E_{ex}[b)]/eV	f_{total}	assignment	E_{ex}[c)]/eV	f	f_{total}
broad band	102.7	0.09	$2p_{3/2} \rightarrow \sigma^*4s(4sa_1)$	103.06	0.05	$2p_{3/2} \rightarrow 3da_1[t_2]$	102.64	0.015	0.085
						$2p_{3/2} \rightarrow 3db_1[t_2]$	102.68	0.014	
	103.4		$2p_{1/2} \rightarrow \sigma^*4s(4sa_1)$	103.66		$2p_{3/2} \rightarrow 3db_2[t_2]$	103.17	0.016	
						$2p_{1/2} \rightarrow 3da_1[t_2]$	103.28	0.008	
						$2p_{1/2} \rightarrow 3db_1[t_2]$	103.32	0.007	
	103.8		$2p_{3/2} \rightarrow \sigma^*(t_2)(3pt_2)$	104.25		$2p_{1/2} \rightarrow 3db_2[t_2]$	103.81	0.009	
						$2p_{3/2} \rightarrow 4sa_1$	103.58	0.011	
	104.4		$2p_{1/2} \rightarrow \sigma^*(t_2)(3pt_2)$	104.85		$2p_{1/2} \rightarrow 4sa_1$	104.22	0.005	
sharp lines	104.9		$2p_{3/2} \rightarrow 5s$	105.47		$2p_{3/2} \rightarrow 3da_1[e]$	104.93		
			$2p_{3/2} \rightarrow 3d(e)$	105.54		$2p_{3/2} \rightarrow 3da_2[e]$	104.93		
	105.5		$2p_{1/2} \rightarrow 5s$	106.07		$2p_{1/2} \rightarrow 3da_1[e]$	105.57		
			$2p_{1/2} \rightarrow 3d(e)$	106.14		$2p_{1/2} \rightarrow 3da_2[e]$	105.57		
			$2p_{3/2} \rightarrow 3d(t_2)$	106.11		$2p_{3/2} \rightarrow 5sa_1$	105.64		
	106.1		$2p_{1/2} \rightarrow 3d(t_2)$	106.71		$2p_{3/2} \rightarrow 4da_1[e]$	106.14		
						$2p_{3/2} \rightarrow 4da_2[e]$	106.14		
						$2p_{1/2} \rightarrow 5sa_1$	106.28		

[a)] From Ref.[2].

[b)] For the CI calculations, $E_{ex} = I^{exp} - (I^{CI} - E^{CI})$, where I^{exp} is the experimental ionization limit of $2p_{1/2}$(107.7 eV) or $2p_{3/2}$(107.1 eV); I^{CI} is the CI calculated Si 2p ionization limit, and E^{CI} is the CI calculated excitation energy.

[c)] For our calculations, E_{ex} of the transition from $2p_{3/2}$ is the average of the excitation energies of the transition from $(2p_{3/2})_1$ and $(2p_{3/2})_2$ (Table 2).

We return to discuss the structures corresponding to transitions into RMOs. Comparing Fig.2(a) with Fig.2(b), with the energy resolution about 0.05 eV the spectra corresponding to transitions into RMOs are relatively insensitive to the geometry of the core-excited molecule. Thus, they can be regarded as fingerprints to determine the geometry of free molecules in their ground state. Note that with further improved energy resolution, the spectra corresponding to transitions into RMOs will also depend on the geometry of the core-excited molecule.

Based on multi-scattering self-consistent field method, our calculated results (see Figs.1 and 2) are encouraging in comparison with the experimental observations. Therefore, with such a starting point, and taking into consideration the channel interactions, further improvement of theoretical treatment, is possible by our recently developed multi-channel theory in atomic systems.[38−40] Specifically, with the fixed molecular geometry, we can calculate the electronic part of eigenchannel parameters and the corresponding eigenchannel wavefunctions. In order to consider the vibronic interactions, we can expand the basis by constructing configuration wavefunctions with various molecular geometries. From such a point of view, to elucidate the structures of a super-excited molecular system,[41] in which molecular dissociation and ionization processes compete with each other, will be our ongoing theoretical effort.

Acknowledgments

The authors would like to express thanks to Mr. X. Kong for some numerical computations. We would also like to thank the referee of this paper for pointing out the coupling between the molecular field effect and the spin–orbit interaction.

Appendix A: the spin–orbit interaction and molecular- field splittings

Both the spin–orbit interactions and the molecular-field effects may cause the energy level splittings in $l \neq 0$ core orbitals.[36,37,42] Børve[36] and Fink[37] have proposed the simple theoretical treatments on the spin–orbit and molecular-field splittings for core-

excited molecules. The spin–orbit interaction Hamiltonian is written as

$$\hat{H}_{\rm SO} = \gamma \cdot \boldsymbol{s} \cdot \boldsymbol{l}, \qquad \text{(A1)}$$

where γ is the spin–orbit parameter, which could be obtained from the observed energy difference $\Delta\epsilon$ between the $J = l + 1/2$ and $J = l - 1/2$ ionization thresholds. For the p orbital, $\Delta\epsilon = \frac{3}{2}\gamma$. The spin–orbit interaction Hamiltonian can be expressed as (for p orbitals)

$$H_{\rm SO} = \frac{\gamma}{2}\begin{pmatrix} 0 & 1 & -1 \\ 1 & 0 & 1 \\ -1 & 1 & 0 \end{pmatrix}, \qquad \text{(A2)}$$

with the basis set of either ($p_x\alpha$, $ip_y\alpha$, $p_z\beta$) or ($p_x\beta$, $-ip_y\beta$, $-p_z\alpha$). Here, p_x, p_y and p_z are the p Cartesian orbitals. Note that two of matrix elements are of different signs from those provided in Ref.[37]. The total Hamiltonian matrix is then written as

$$H = \begin{pmatrix} \epsilon_x & \gamma/2 & -\gamma/2 \\ \gamma/2 & \epsilon_y & \gamma/2 \\ -\gamma/2 & \gamma/2 & \epsilon_z \end{pmatrix}, \qquad \text{(A3)}$$

where ϵ_x, ϵ_y and ϵ_z are the orbital energies of the p_x, p_y and p_z orbitals respectively; and the molecular-field effects are included. Diagonalization of the matrix leads to the eigenvalues and eigenvectors that represent the molecular p core orbitals.

For the SiH_4 molecule with a $T_{\rm d}$ symmetry, the Si $2p_x$, $2p_y$ and $2p_z$ core orbitals are degenerate $1t_2$ molecular orbitals. Thus, we have $\epsilon_x = \epsilon_y = \epsilon_z$, and diagonalizing matrix (A3) leads to the following eigenvectors:

$$|2p_{1/2,1/2^+_-}\rangle = \frac{1}{\sqrt{3}}|2p_{x\beta}^{\alpha}\rangle \mp \frac{i}{\sqrt{3}}|2p_{y\beta}^{\alpha}\rangle \pm \frac{1}{\sqrt{3}}|2p_{z\alpha}^{\beta}\rangle,$$

$$|2p_{3/2,1/2^+_-}\rangle = -\frac{1}{\sqrt{6}}|2p_{x\beta}^{\alpha}\rangle \pm \frac{i}{\sqrt{6}}|2p_{y\beta}^{\alpha}\rangle \pm \sqrt{\frac{2}{3}}|2p_{z\alpha}^{\beta}\rangle,$$

$$|2p_{3/2,3/2^+_-}\rangle = \frac{1}{\sqrt{2}}|2p_{x\beta}^{\alpha}\rangle \pm \frac{i}{\sqrt{2}}|2p_{y\beta}^{\alpha}\rangle. \qquad \text{(A4)}$$

Here, we adopt the S_4 axis as the $\hat{z}$ axis. The symbol $2p_{J,|M_J|}$ denotes the orbital whose total angular momentum is J and its projection on the $\hat{z}$ axis is M_J. For a C_{2v} symmetry, the C_2 axis (corresponding to the S_4 axis of a $T_{\rm d}$ symmetry) is adopted as the $\hat{z}$ axis. The Si $2p_x(b_1)$, $2p_y(b_2)$ and $2p_z(a_1)$ core orbitals are no longer degenerate. Their energies can be calculated with HF/6-311++G** using the Gaussian 98 program.[43] The differences of the calculated energies are $\epsilon_y - \epsilon_z = -0.02$eV and $\epsilon_x - \epsilon_z = 0.03$eV. We can obtain γ from the observed spin–orbit splitting of the Si 2p thresholds $\Delta\epsilon$ by $\gamma = \frac{2}{3}\Delta\epsilon = 0.43$eV. Then, diagonalizing matrix (A3) leads to the Si 2p core orbitals with spin–orbit and molecular-field splittings of a C_{2v} symmetry.

References

[1] Kern W and Ban V S 1978 *Thin Film Process*, Vossen J L and Kern W, ed (New York: Academic) p257

[2] Friedrich H, Sonntag B, Rabe P, Butscher W and Schwarz W H E 1979 *Chem. Phys. Lett.* **64** 360

[3] Cooper G, Ibuki T and Brion C E 1990 *Chem. Phys.* **140** 147

[4] Cooper G, Burton G R, Chan W F and Brion C E 1995 *Chem. Phys.* **196** 293

[5] Sutherland D G J, Bancroft G M, Bozek J D and Tan K H 1992 *Chem. Phys. Lett.* **199** 341

[6] Puttner R, Domke M, Lentz D and Kaindl G 1997 *Phys. Rev.* A **56** 1228

[7] Johnson K H, 1973 *Scattered-wave theory of the chemical bond, Adv. Quant. Chem.* 7 ed. P O Lowdin (New York: Academic) p143

[8] Dill D and Dehmer J L 1974 *J. Chem. Phys.* **61** 692

[9] Liang X L, Pan X C and Li J M 1985 *Chin. Phys. Lett.* **2** 545

[10] Pan X C, Liang X L and Li J M 1987 *Acta Phys. Sin.* **36** 426

[11] Liu L and Li J M 1991 *J. Phys. B: At. Mol. Opt. Phys.* **24** 1893

[12] Zhang P H and Li J M 1996 *Phys. Rev.* A **54** 665

[13] Zhang Y, Zhang P H and Li J M 1997 *Phys. Rev.* A **56** 1819

[14] Niu A F, Zhang Y, Zhang W H and Li J M 1998 *Phys. Rev.* A **57** 1912

[15] Zhang W H, Zhong Z P and Li J M 2000 *Sci. Chin.* A **43** 871

[16] Li J M in 1986 *Electronic and Atomic Collisions*, ed. Lorents D C, Meyerhof W E, Peterson J R (Amsterdam: Elsevier) p621

[17] Zhong Z P, Zhang W H, Xu K Z, Feng R F and Li J M 1999 *Phys. Rev.* A **60** 236

[18] Tong X M and Li J M 1991 *J. Phys. B: At. Mol. Opt. Phys.* **24** 1893

[19] Fano U 1970 *Phys. Rev.* A **2** 353

[20] Lee C M (Li J M) 1977 *Phys. Rev.* A **6** 109

[21] Jungen C and Atabek O 1977 *J. Chem. Phys.* **66** 5584

[22] Guo W L, Liang X L and Li J M 1986 *Chin. Phys. Lett.* **3** 441

[23] Li J M 1987 *Atomic Physics* 10, ed Narumi H, Shimamura I (Amsterdam: Elsevier) p303

[24] Liu L and Li J M 1991 *Chin. Phys. Lett.* **8** 129

[25] Liu L and Li J M 1991 *J. Phys. B: At. Mol. Opt. Phys.* **24** 1893
[26] Yang H W, Liu L and Li J M 1992 *Acta Phys. Sin.* **41** 10
[27] Yang H W, Sun B and Li J M 1992 *Chin. Phys. Lett.* **9** 133
[28] Sun B and Li J M 1992 *Acta Phys. Sin.* **41** 853
[29] Sun B and Li J M 1993 *Acta Phys. Sin.* **42** 25 (in Chinese)
[30] (a) Sze K H, Brion C E, Tong X M and Li J M 1987 *Chem. Phys.* **115** 433
(b) Tong X M, Li J M, Sze K H and Brion C E, in 1987 *14th Int. Conf. on x-ray & Inner-shell Processes (Paris, France)*
[31] Tong X M and Li J M 1989 *J. Phys. B: At. Mol. Opt. Phys.* **22** 1531; in 1989 *16th Int. Conf. on Photonic, Electronic and Atomic Collisions (New York)* p6
[32] Bao M Q, Tong X M and Li J M 1989 *Chin. J. Chem. Phys.* **2** 427
[33] Tong X M and Li J M 1989 *Acta Phys. Sin.* **38** 1951 (in Chinese)
[34] Zhang W, Sze K H, Brion C E, Tong X M and Li J M 1990 *Chem. Phys.* **140** 265
[35] Zhong Z P, Zhang W H and Li J M 2000 *J. Chem. Phys.* **113** 316
[36] Børve K J 1996 *Chem. Phys. Lett.* **262** 801
[37] Fink R F 1998 *Phys. Rev.* A **58** 1988
[38] Zou Y, Tong X M and Li J M 1995 *Acta Phys. Sin.* **44** 50 (in Chinese)
[39] Huang W, Zou Y, Tong X M and Li J M 1995 *Phys. Rev.* A **52** 2770
[40] Tong X M, Zou Y and Li J M 1995 *Chin. Phys. Lett.* **12** 351
[41] Lee C M (Li J M) 1977 *Phys. Rev.* A **16** 109
[42] Hudson E, Shirley D A, Domke M, Remmers G and Kaindl G 1994 *Phys. Rev.* A **49** 161
[43] Frisch M J *et al* 1998 Gaussian 98, Revision A.3, (Gaussian, Inc., Pittsburgh PA)